Dipolar and Ionic Relaxations of Polymers Containing Polar Conformationally Versatile Side Chains

ARTICLE *in* MACROMOLECULES · JUNE 2010

Impact Factor: 5.8 · DOI: 10.1021/ma1004875

5 AUTHORS, INCLUDING:

M.J. Sanchis
Universitat Politècnica de València
106 PUBLICATIONS **869** CITATIONS
SEE PROFILE

Pilar Ortiz-Serna
Universitat Politècnica de València
17 PUBLICATIONS **51** CITATIONS
SEE PROFILE

Gustavo. Dominguez-Espinosa
Laboratorio Tecnologico del Uruguay (LATU)
11 PUBLICATIONS **106** CITATIONS
SEE PROFILE

Ricardo Díaz-Calleja
Universitat Politècnica de València
223 PUBLICATIONS **1,720** CITATIONS
SEE PROFILE

Macromolecules
ARTICLE

Macromolecules **2010**, *43*, 5723–5733 **5723**
DOI: 10.1021/ma1004875

Dipolar and Ionic Relaxations of Polymers Containing Polar Conformationally Versatile Side Chains

M. J. Sanchis, M. Carsí, P. Ortiz-Serna, G. Domínguez-Espinosa, and R. Díaz-Calleja*

Instituto de Tecnología Eléctrica, ITE, ETSII, Universidad Politécnica de Valencia, Valencia, Spain

E. Riande*

Instituto de Ciencia y Tecnología de Polímeros (CSIC) Juan de la Cierva 3, 28003, Madrid, Spain

L. Alegría, L. Gargallo, and D. Radić

Departamento de Química Física, Pontificia Universidad Católica de Chile, Santiago, Chile

Received March 5, 2010; Revised Manuscript Received June 2, 2010

ABSTRACT: This work reports a comparative study of the response of poly(2,3-dimethoxybenzyl methacrylate), poly(2,5-dimethoxybenzyl methacrylate), and poly(3,4-dimethoxybenzyl methacrylate) to electrical perturbation fields over wide frequency and temperature windows with the aim of investigating the influence of the location of the dimethoxy substituents in the phenyl moieties on the relaxation behavior of the polymers. The dielectric loss isotherms above T_g exhibit a blurred relaxation resulting from the overlapping of secondary relaxations with the glass−rubber or α relaxation. At high temperatures and low frequencies, the α relaxation is hidden by the ionic conductive contribution to the dielectric loss. As usual, the real component of the complex dielectric permittivity in the frequency domain increases with decreasing frequency until a plateau is reached corresponding to the glass−rubber (α) relaxation. However, at high temperatures, the real permittivity starts to increase again with decreasing frequency until a second plateau is reached, a process that presumably reflects a distributed Maxwell−Wagner−Sillars relaxation or α′ absorption. The α and α′ processes appear respectively as asymmetric and symmetric relaxations in the loss electrical modulus isotherms in the frequency domain. To facilitate the deconvolution of the overlapping absorptions, the time retardation spectra of the polymers were computed from the complex dielectric permittivity in the frequency domain using linear programming regularization parameter techniques. The spectra exhibit three secondary absorptions named, in increasing order of time γ', γ, and β followed by the α relaxation. At long times and well separated from the α absorption the α′ relaxation appears. The replacement of the hydrogen of the phenyl group in position 2 by the oxymethyl moiety enhances the dielectric activity of the poly(dimethoxybenzyl methacrylate)s. The temperature dependence of the relaxation times associated with the different relaxations is studied, and the molecular origin of the secondary relaxations is qualitatively discussed.

1. Introduction

Owing to the rich dynamics of poly(*n*-alkyl methacrylate)s, the relaxation processes of a series of these polymers have been studied using different experimental techniques involving dielectric and NMR spectroscopies, dynamic mechanical analysis, dilatometry, and modulated calorimetry.[1−15] Many of these studies have been focused on both the evolution of the relaxation processes of the homologous series of polymethacrylates with side chains length and the crossover region where the α and β relaxations merge to form a single $\alpha\beta$ absorption.[10−13,16−18] On the basis of the fact that the β absorption is a thermally activated process whereas the glass−rubber or α relaxation also depends on the free volume, as earlier as in the 1960s Williams[19] studied the influence of pressure on the relaxation behavior of polymers, finding that merging of the α and β relaxations to form the $\alpha\beta$ process takes place as temperature is raised, at ambient pressure, and demerging is accomplished by application of a hydrostatic pressure. Recently, Mpoukouvalas et al.[15] derived the canonical equations that describe the effects of the thermodynamic variables P, V, T on the average relaxation times in poly(ethyl methacrylate). These authors found that although both intra- and intermolecular interactions, controlled respectively by temperature and volume, contribute to the α relaxation, it is the temperature variable that exerts the stronger influence; in fact, without thermal energy relaxations could not occur at all. Moreover, the study of the activated volume reveals that the $\alpha\beta$ relaxation presents the characteristics of a segmental process and not the characteristics of the local β absorption whose apparent activation volume is much smaller.

Dielectric activity in poly(*n*-alkyl methacrylate)s arises from motions of the dipole moment associated with the side ester moiety of the repeating units.[9,15,16] The α relaxation is produced by motions of dipole components μ_b rigidly attached to the chain backbone which move when cooperative motions of the backbone occurs. Before the crossover region, the dipoles components μ_s in the flexible side groups move independently or in concert with local motions of the backbone, giving rise to the β relaxation. Above coalescence the side groups move in concert with the overall motions of the backbone, giving the $\alpha\beta$ process. In spite of

*To whom correspondence should be addressed.

Published on Web 06/14/2010

the nonpolarity of the alkyl residues, the dynamics of the chains of poly(*n*-alkyl methacrylate)s in the liquid rubbery state is strongly dependent on the number of methylene groups of the alkyl residue. A great deal of work has been mainly focused on the crossover region of the dynamic glass transition where the α relaxation and the β mode approach each other. At high temperature, a process appears above the crossover different from the cooperative α relaxation operative below the crossover. In principle, an increase in chains length increases the free volume shifting this scenario to lower frequency and temperature. An important discovery in these studies is the nanophase separation of incompatible main- and side-chain parts of the higher members of the poly(*n*-alkyl methacrylate)s series.[10,20] The existence of two dynamic glass transitions for the higher members of the series, the conventional α process, and an additional low-temperature glass transition α_{PE}, is put in evidence in shear measurements carried out in combination with dielectric, calorimetric, and WAXS data.[10] The α_{PE} absorption is related to cooperative motions of the polyethylene-like side-chain parts whereas the α relaxation arises from segmental motions of the chains backbone flanking the nanodomains. The presence of static monodomains in the range 0.5−1.5 nm is confirmed by X-ray scattering data.[10]

Despite the great amount of work reported in the literature on the dynamics of poly(*n*-alkyl methacrylate)s, relatively little work deals with the dynamics of poly(methacrylate)s with alcohol residues containing polar moieties in their structure. Recent experiments[21−26] carried out on the relaxations of poly(benzyl methacylate)s show that changes in the location of polar atoms replacing hydrogen atoms in the phenyl group greatly affects the relaxation behavior of the polymers. For example, the dynamics of poly(benzyl methacylate)s in which hydrogen atoms of the phenyl groups are replaced by halogen atoms is strongly dependent not only on the degree of substitution and nature of the halogen atoms but also on the location of the substitutions. Preliminary studies carried out in our laboratories focused on the response of poly(2,3-dimethoxybenzyl methacrylate) (PDBM23) to electrical perturbation fields showed that the isochrone at 1 Hz of the real component ε' of the complex dielectric permitivitty ε^* apparently exhibits two maxima centered respectively at 45 and 100 °C. The two maxima might be associated with the existence of polar and nonpolar nanodomains formed respectively by polar side groups of the chains and the nonpolar backbone. Another possibility is that the lower temperature maximum corresponds to the glass−rubber relaxation whereas the second one could be attributed to charge transport. It must be emphasized that as a consequence of the conductivity response, the high-temperature maximum observed in the isochrone ε' is not detected in the dielectric loss isotherms. This at first sight anomalous dielectric behavior prompted us to study in detail the relaxation behavior of PDBM23, paying special attention to the processes of charge transport detected at low frequencies and high temperatures. Another objective of this work was to carry out a comparative study of the dielectric behavior of poly(2,3-dimethoxybenzyl methacrylate) with that of poly(2,5-dimethoxybenzyl methacrylate) (PDBM25) and poly(3,4-dimethoxybenzyl methacrylate) (PDBM34) with the aim of assessing how the locations of the oxymethylene moieties affect dipolar relaxations and ionic transport.

2. Experimental Part

Synthesis and Characterization of the Monomers. The monomers 2,3-dimethoxybenzyl-, 2,5-dimethoxybenzyl, and 3,4-dimethoxybenzyl methacrylates were obtained respectively by reaction of methacryloyl chloride with 2,3-dimthoxybenzyl alcohol, 2,5-dimethoxybenzyl alcohol, and 3,4-dimethoxybenzyl alcohol at reflux temperature using toluene as solvent following the procedure of Burtle et al.[27] improved by Gargallo et al.[28] The

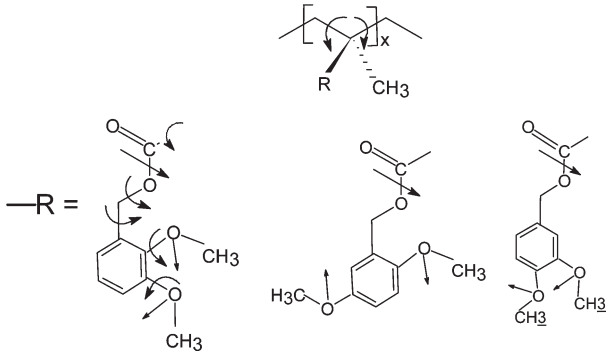

Figure 1. From left to right schemes of the planar structures of the side chains of PDBM23, PDBM25, and PDBM34. As an example, rotations that may produce dielectric activity are indicated in the scheme of PDBM23 and the backbone (top). Notice that the C(O)−O bond is planar; i.e., it is restricted to the trans state. Arrows indicate dipole moments associated with polar moieties of the side chains.

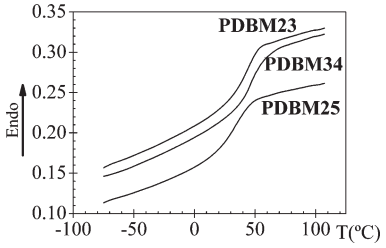

Figure 2. DSC thermograms corresponding to the PDBM23, PDBM25, and PDBMA34.

monomers were isolated and purified at reduced pressure (80°−95°, 1 mmHg). The purity of the monomers was checked by ^{1}H NMR spectroscopy (see Supporting Information).

Synthesis and Characterization of the Polymers. Polymerization reactions of the respective monomers were carried out at 50 °C in toluene solutions, under a nitrogen atmosphere, using α,α′-azobis(isobutyronitrile) (AIBN) as initiator. Polymers were precipitated with methanol, dissolved in chloroform, precipitated again with methanol, and dried in a vacuum oven at 60 °C. The purity of the polymers was checked by ^{1}H NMR spectroscopy (see Supporting Information). The weight-average molecular weights of the polymers determined by GPC were 1.4×10^5, 2.1×10^5, and 1.7×10^5 for PDBM23, PDBM25, and PDBM34, respectively, and the molecular weight heterodispersity index was about 1.8. The stereochemical structure of the samples as determined by NMR was atactic. The repeating units of the polymers are shown in Figure 1.

DSC Measurements. The glass transition temperature was measured with a TA DSC-Q10 apparatus at a heating rate of 10 °C/min, under a nitrogen atmosphere, and the pertinent thermograms obtained in the second run are shown in Figure 2. The glass transition temperatures of PDBM23, PDBM25, and PDBM34, estimated as the temperature at the midpoint of the endotherms, were 47, 37, and 57 °C, respectively.

X-ray Characterization. Wide-angle X-ray diffraction (WAXS) patterns were recorded at room temperature using a Bruker D8 Advance diffractometer with Cu Kα radiation (λ = 0.1542 nm) operated at 40 kV and 4 mA. The diffraction scans were collected within the range of 2θ = 5°−60° with a 2θ step of 0.024° and 0.5 s per step.

Dielectric Measurements. The complex dielectric permittivity of the samples was measured with a Novocontrol broadband dielectric spectrometer (Hundsagen, Germany) integrated by a SR 830 lock-in amplifier with an Alpha dielectric interface an Agilent 4991 coaxial line reflectometer to carry out the measurement in the frequency range 10^{-1}−10^6 and 10^6−10^9 Hz, respectively. In the latter case the complex permittivity was obtained by measuring the

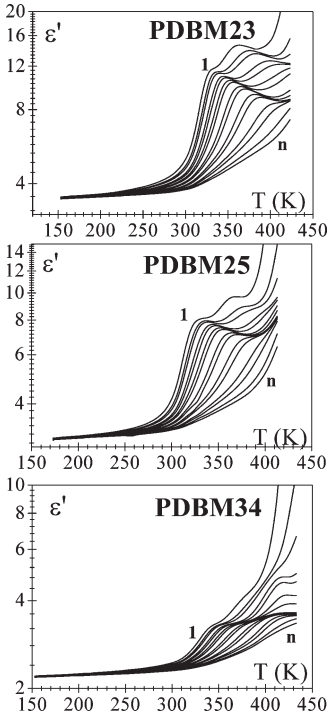

Figure 3. Dielectric permittivity as a function of temperature for PDBM25, PDBM23, and PDBM34 at several frequencies: 1.09×10^{-1}, 5.37×10^{-1}, 1.19, 5.86, 1.3×10^{1}, 4.29×10^{1}, 9.52×10^{1}, 4.69×10^{2}, 1.04×10^{3}, 5.12×10^{3}, 1.13×10^{4}, $5 \times 58 \times 10^{4}$, 1.24×10^{5}, 4.09×10^{5}, and 9.08×10^{5} Hz.

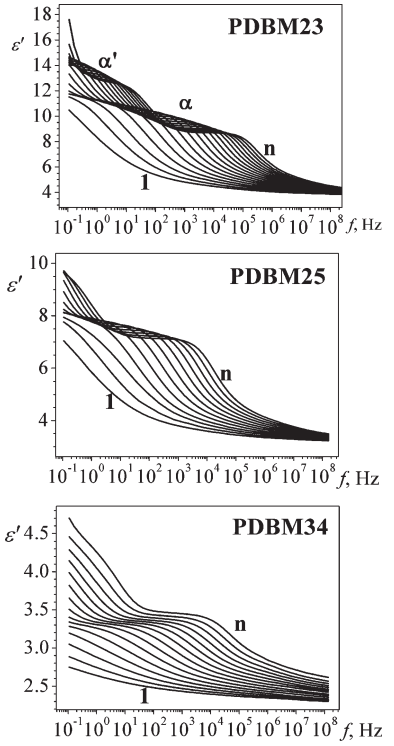

Figure 4. Dielectric permittivity in the frequency domain for PDBM23, PDBM25, and PDBM34 in the temperature ranges 323−408, 318−373, and 323−393 K, respectively, at 5 K steps.

reflection coefficient at a particular reference plane. The electrodes used were gold disks of 20 and 10 cm for the measurements carried out in the range $10^{-1}-10^{6}$ and $10^{6} - 10^{9}$ Hz, respectively. The temperature was controlled by a nitrogen jet (QUATRO from Novocontrol) with a temperature error of 0.1 K during every single sweep in frequency.

3. Results

Isochrones showing the variation of the real component ε' of the dielectric complex permittivity ε^* of the polymers with temperature, at several frequencies, are shown in Figure 3. All the isochrones display the same pattern in the sense that they present two steps: a low-temperature step associated with the glass rubber or α relaxation followed by a second step at higher temperature, named the α′ absorption, whose nature will be discussed later. The isochrones corresponding to the dielectric loss ε'' present an ostensible α relaxation followed by a rather sharp increase of the loss as temperature increases as a result of the strong contribution of the conductivity to ε'' . It is worth noting that in the low-temperature side of the glass−rubber (α) relaxation a shoulder appears, corresponding to a secondary relaxation, presumably the β process associated with side chain motions. For details see Figure 1 of the Supporting Information.

Isotherms for ε' in the frequency domain corresponding to PDBM23, PDBM25, and PDBM34, at several temperatures, are shown in Figure 4. Let us focus on the isotherms corresponding to PDBM23. As usual, ε' increases as frequency decreases, reaching a plateau corresponding to the relaxed dipoles. However, after the plateau and as frequency decreases further, ε' increases again, reaching a second plateau. The two rather steeply changes in the values of ε' correspond in the order of decreasing frequency to the α and α′ relaxations detected in the isochrones of ε' in Figure 2. The isotherms of PDBM25 and PDBM34 present the same pattern as those of PDBM23, though to reach the second plateau would require data obtained at lower frequencies than those used in this study.

The dielectric loss isotherms in the frequency domain, shown in Figure 5, do not present well-defined relaxations in the high-frequency regions. However, they exhibit an ostensible relaxation associated with the glass−rubber relaxation which at higher temperatures and lower frequencies is apparently hidden by the conductive contribution. Better definitions of the loss peaks are obtained by plotting the dielectric results in terms of the dielectric loss modulus, M''. The isotherms of M'' in the frequency domain, shown in Figure 6, exhibit two ostensible peaks corresponding in decreasing order of frequency to the α and α′ relaxations. The isotherms at different temperatures for M', the real component of the complex dielectric modulus M^* of the polymers, are shown in Figure 2 of the Supporting Information. In all the cases the modulus increases with frequency, reaching a plateau corresponding to the α relaxation, and then the modulus increases again until a second plateau corresponding to the α′ relaxation process.

Retardation Spectra. The isotherms for ε' in frequency domain corresponding to PDBM23 clearly show the presence of two ostensible relaxations at $T > T_g$ so that $\varepsilon^*(\omega)$ can be written as

$$\varepsilon^*(\omega) = \varepsilon_\infty + \sum_{\substack{i,\,\text{second.}\\ \text{absorp}}} \frac{\varepsilon_{0i} - \varepsilon_{\infty i}}{1 + (j\omega\tau_{si})^{a_{si}}} + \frac{\varepsilon_{0\alpha} - \varepsilon_{\infty\alpha}}{[1 + (j\omega\tau_\alpha)^{a_\alpha}]^{b_\alpha}} + \frac{\varepsilon_{0\alpha'} - \varepsilon_{\infty\alpha'}}{1 + (j\omega\tau_{\alpha'})^{a_{\alpha'}}} - j\frac{\sigma}{\varepsilon_f\omega} \quad (1)$$

where ε_f (= 8.854 pF/m) is the free space dielectric permittivity and σ is the ionic conductivity arising from interfacial polymer−electrode phenomena. The subscript i in eq 1 refers to secondary absorptions (β, γ, ...) not well-defined in the dielectric loss spectra whereas the subscripts 0 and ∞ mean respectively relaxed and unrelaxed dielectric permittivities.

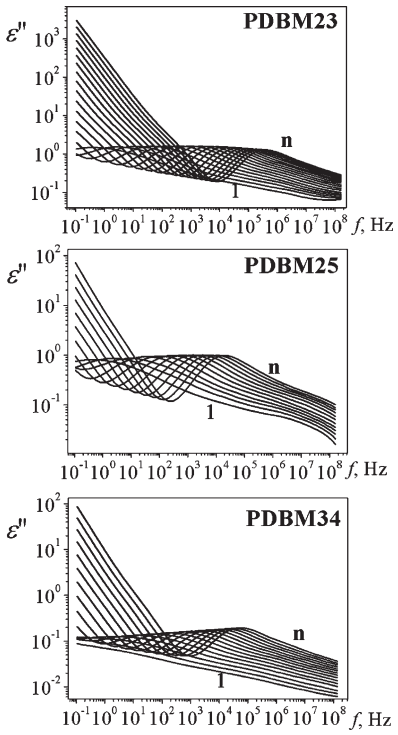

Figure 5. Dielectric loss in the frequency domain for PDBM23, PDBM25, and PDBM34 in the temperature ranges 323−408, 318−373, and 323−393 K, respectively, at 5 K steps.

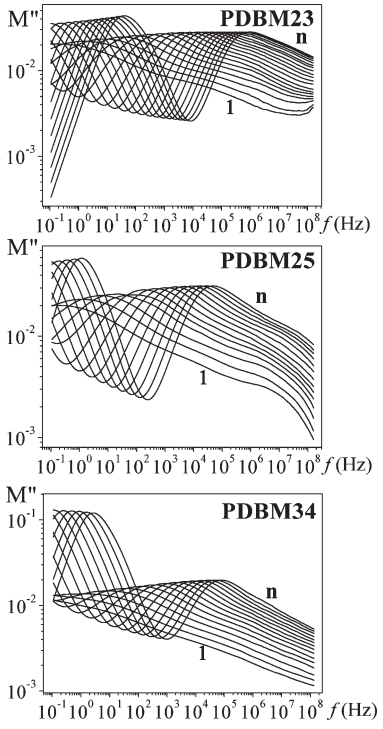

Figure 6. Dielectric loss modulus M'' in the frequency domain for PDBM23, PDBM25, and PDBM34 in the temperature ranges 323−408, 318−373, and 323−393 K, respectively, at 5 K steps.

The shape parameters a and b are related respectively to the departure of the complex ε'' vs ε' plot from a semicircumference, at low frequencies, and to the skewness of the plot along a straight line, at high frequencies.[29] Owing to the symmetry of the secondary absorptions and that of the α′ relaxation observed in the M'' curves in the frequency domain, the complex plots are arcs so that the shape parameter b is the unit. For a Debye type relaxation $a = b = 1$. Deconvolutions of overlapping relaxations are usually carried out utilizing eq 1. However, relaxations are better defined in the retardation spectra than in the dielectric loss spectra in the frequency domain owing to the fact that a Debye relaxation in the frequency domain covers 2.29 decades whereas in the relaxation spectrum is a delta of Dirac. As a result, time retardation spectra facilitate deconvolutions of overlapping relaxations. The complex dielectric permittivity can be expressed in terms of the retardation spectra by[30,31]

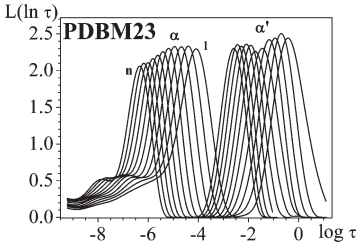

Figure 7. Retardation spectra for PDBM23 in the temperature range 358−408 K, at 5 K steps.

$$\varepsilon^*(\omega) - \varepsilon_\infty = (\varepsilon_0 - \varepsilon_\infty)\int_{-\infty}^{\infty} L(\ln\tau)\frac{1}{1+j\omega\tau}\,\mathrm{d}\ln\tau + \frac{\sigma}{j\omega\varepsilon_\mathrm{f}} \tag{2}$$

where L is the normalized time retardation spectrum. For a frequency ω_i the retardation spectrum can be written in discrete form, and eq 2 can approximately be written as

$$\varepsilon^*(\omega_i) - \varepsilon_\infty \cong \sum_{k=1}^{N} R^*_{ik} L_k + \frac{\sigma}{j\omega_i\varepsilon_\mathrm{f}} \tag{3}$$

where

$$R^*_{ik} = \frac{\Delta\ln\tau_k}{1+j\omega_i\tau_k} \tag{4}$$

and $L_k = (\varepsilon_0 - \varepsilon_\infty)L(\ln\tau_k)$. The computation of the retardation spectra of the polymers can be accomplished by minimization of the error function[32]

$$E = \sum_{i=1}^{N}\left\{\varepsilon(\omega_i) - \sum_{k=1}^{N'} R^*_{ik}L_k - \frac{\sigma}{j\omega\varepsilon_\mathrm{f}} - \varepsilon_\infty\right\}^2 \tag{5}$$

Owing to the ill-conditioned behavior of the error function, the Tikhonov[33] regularization technique was used to minimize E. The pertinent steps to carry out the minimization that leads to the calculation of the retardation spectrum were described in detail elsewhere.[32]

The retardation spectrum of PDBM23, shown in Figure 7, exhibits two ostensible peaks corresponding in increasing order of time to the α and α′ relaxations. In addition, three secondary absorptions can be detected at short times called in order of decreasing time β, γ, and γ'. The retardation spectra are strongly sensitive to the location of the dimethoxy moieties in the phenyl group of the alcohol residue as the retardation spectra of PDBM23, PDBM25, and PDBM34, presented at a single temperature in Figure 8, show. It can be seen that the intensities of the α and α′ relaxation peaks increase in the order PDBM23 > PDBM25 > PDBM34.

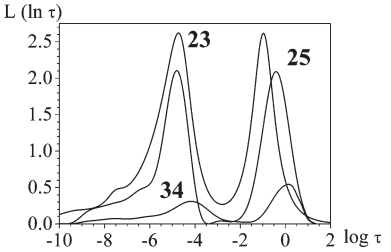

Figure 8. Retardation spectra for PDBM25, PDBM23, and PDBM34 at 368 K.

Deconvolutions of the retardation spectra can be carried out by using the analytical retardation spectra for HN type equations given by[31,34,35]

$$L_i(\ln \tau) = \frac{1}{\pi} \frac{\Delta\varepsilon_i (\tau/\tau_{\mathrm{HN};i})^{a_i b_i} \sin b_i\theta_i}{\left[(\tau/\tau_{\mathrm{HN};i})^{2a_i} + 2(\tau/\tau_{\mathrm{HN};i})^{a_i} \cos a_i\pi + 1\right]^{b_i/2}} \tag{6}$$

In this expression, $0 < a_i\, b_i \leq 1$ and θ_i is given by

$$\theta_i = \arctan\left[\frac{\sin \pi a_i}{(\tau/\tau_{\mathrm{HN};i})^{a_i} + \cos \pi a_i}\right] + c \tag{7}$$

where c is 0 or π if the argument of the arctan function is respectively positive or negative[17] and i denotes the relaxation (γ', γ, β, α, α'). The parameter $\Delta\varepsilon_i = \varepsilon_{0i} - \varepsilon_{\infty i}$ is the strength of the relaxation i. Owing to the fact that the degree of overlapping between α and α' relaxations is rather small at most temperatures, the α' relaxation was deconvoluted from the spectrum first. In an initial step, the fitting procedure was carried out using partial parts of the retardation spectrum as briefly described below. The high time side of the α relaxation was used as reference for the deconvolution of this process; once separated, the α relaxation, the high time side of the spectrum was used to deconvolute the β relaxation and so on. Once obtained the starting parameters, we proceeded to deconvolute the global spectrum delimiting, in the fitting procedure, the values of HN parameters for each relaxation in a range that includes the preliminary adjustment parameters, with the condition that $0 < a_i, b_i \leq 1$, and the sum of the dielectric strengths of the relaxations is equal to the global dielectric strength calculated by means of the expression $\varepsilon_0 - \varepsilon_\infty = \int_{-\infty}^{\infty} L(\ln \tau)\, \mathrm{d} \ln \tau$. Finally, the deconvolutions were refined by slightly changing the parameters until the difference between the original spectrum and that obtained from the deconvolutions using the expression $L(\ln \tau) = \sum_{i=1}^{4} L_i(\ln \tau)$ is lower than 2% for any retardation time.

The retardation spectra for the relaxations γ', γ, β, α, and α' of PDBM23, at 16 temperatures, are presented in Figure 9. The deconvoluted spectra of these relaxations for PDBM25 and PDBM34 are shown in Figures 3 and 4 of the Supporting Information. An inspection of Figure 9 shows that the α and β relaxations coexist in the range of temperatures $T_g < T <$ 365 K; then the β process is apparently swallowed by the α relaxation forming a single relaxation. The strength of the relaxations can directly be obtained from the deconvoluted spectra by means of the following expression

$$\varepsilon_{0i} - \varepsilon_{\infty i} = \int_{-\infty}^{\infty} L_i(\ln \tau) \mathrm{d} \ln \tau \tag{8}$$

where i denotes the type of relaxation (γ', γ, β, α, and α'). Values of the strength for PDBM23, PDBM25, and PDBM34 are plotted as a function of the reciprocal of temperature in Figure 10. The strength of the α relaxation of PDBM23 decreases with increasing temperatures, whereas that of the β increases until a temperature is reached at which both relaxations have the same strength. At this temperature both relaxations form a single absorption whose strength rises steeply and then decreases as temperature increases. The evolution of the strengths of the α and β relaxations with temperature for PDBM34 is similar to that of PDBM23 in the sense that both processes form a single absorption at the same temperature, though the strength of the β relaxation at this temperature is lower than that of the α. For PDBM25, the strength of the α relaxation decreases with increasing temperature whereas that of the β increases becoming equal to that of the α at 373 K. The strength of the α' relaxation of PDBM23 decreases with increasing temperature, varying from 4.27 at 358 K to 3.09 at 408 K. The α' relaxations of PDBM25 and PDBM34 are only observable at a reduced number of temperatures. The data available indicate that the strength of the α' relaxation of PDBM25 is somewhat smaller than that of PDBM23, whereas that of PDBM34 is significantly smaller than the strength of the α' relaxation of PDBM23. The strengths of the γ and γ' relaxations are significantly lower than those of the β process, independently of the polymer considered. The total dielectric strength of the dipolar processes calculated from the retardation spectra follows the trends $\Delta\varepsilon$(PDBM23) ≥ $\Delta\varepsilon$(PDBM25) > $\Delta\varepsilon$(PDBM34), in agreement with the results of Figure 4.

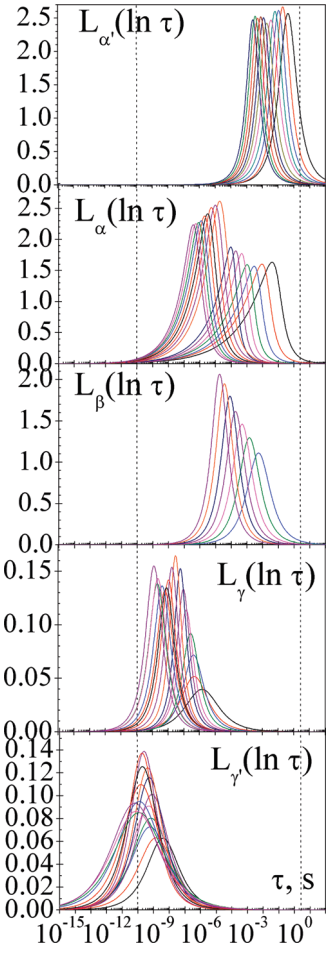

Figure 9. Retardation spectra for PDBM23 corresponding to α', α, β, γ, and γ' processes (318−408 K, at 5 K steps). The dashed lines indicate that out of the limits the values of $L_i(\ln \tau)$ should be regarded as approximate.

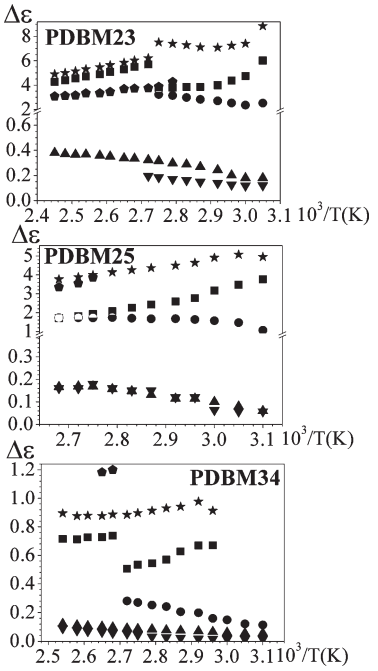

Figure 10. Temperature dependence of the strengths of the α′ (pentagons), α (squares), β (circles), γ (up triangles), and γ' (down triangles) relaxations. Star symbols represent the total dipolar dielectric strength.

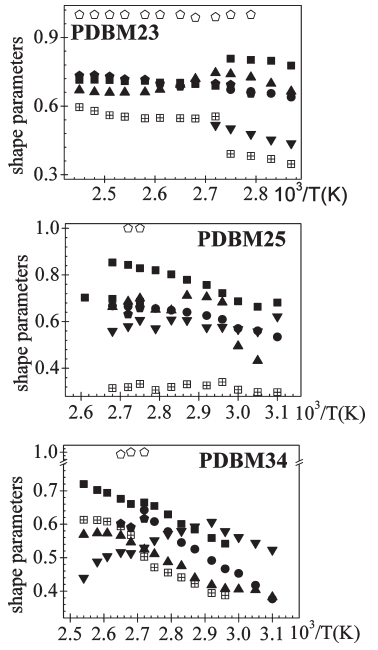

Figure 11. Temperature dependence of the shape parameters (a_k, b_k) for the α′ (■), α (▲), β (▼), γ (⊞), and γ' (⬠) relaxations for PDBM23, PDBM25, and PDBM34.

The shape parameters for the retardation spectra associated with the relaxations are shown as a function of temperature in Figure 11. The value of a for the α relaxation, higher than that for the β process, moderately increases with increasing temperature. However, the parameter a for PDBM23 steeply decreases in the vicinity of 368 K and then slightly increases as temperature goes up. This parameter also increases with temperature for the β and γ relaxations, though for this latter process a undergoes a moderate decrease as temperature increases. The values of a do not

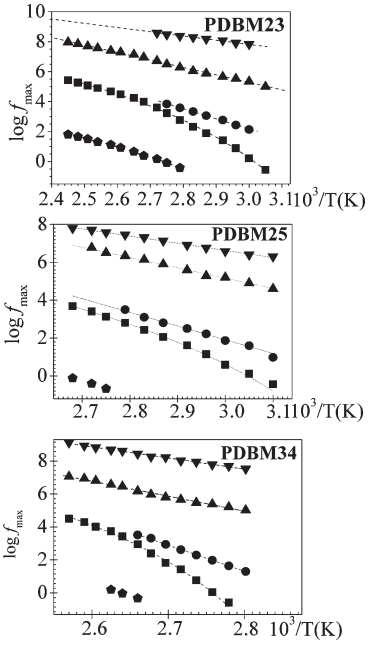

Figure 12. Arrhenius plot for the α′ (pentagons), α (squares), β (circles), γ (up triangles), and γ' (down triangles) relaxations of PDBM25, PDBM23, and PDBM34.

follow a definite trend for the γ' absorption. For PDBM23, the b parameter related with the skewness of the ε'' vs ε' plot in the α relaxation rises steeply in the vicinity of 368 K; below and above this temperature, b slightly increases with temperature. For PDBM25, the value of b is rather low and nearly independent of temperature, whereas the variation of b with temperature for PDBM34 follows similar trends as for PDBM25, though the change in the vicinity of 368 K is somewhat smaller. Finally, the plots of Figure 11 show that the shape parameter b for the α′ relaxation lies in the vicinity of the unit in the whole temperature range, suggesting that the absorption in the retardation spectra is symmetric.

Temperature Dependence of Retardation Times. Arrhenius plots for the secondary absorptions and the α relaxation are plotted in Figure 12. The activation energies E_a of the secondary absorptions are obtained from the slope of the plots, and the pertinent values are given in Table 1. In general, the values of the activation energy of the relaxations follow the trends $E_a(\beta) > E_a(\gamma) > E_a(\gamma')$. Moreover, the activation energies of the γ and γ' relaxations vary in the way E_a(PDBM25) > E_a(PDBM23) > E_a(PDBM34). In the case of the β relaxation, E_a(PDBM34) > E_a(PDBM25) > E_a(PDBM23). As usual, the average relaxation time associated with the α relaxation is described by the Vogel−Fulcher−Tammann−Hesse (VFTH) equation[36−38] expressed in terms of the fragility parameter D_0[39,40] by

$$\tau = \tau_0 \exp\left[\frac{D_0}{(T/T_V)-1}\right] \qquad (9)$$

where τ_0 is a prefactor of the order of picoseconds and T_V is the Vogel temperature currently associated with the temperature at which the entropies of the glassy system and the crystal are similar; i.e., the configurational entropy of the glassy system is nil. Values of the parameters that fit eq 9 to the experimental results are collected in Table 1. The results show that D_0 is lower than 10, the limit value which separates fragile materials (D_0 < 10) from strong ones (D_0 > 10).[39,40] It is

Table 1. Activation Energies of the Secondary Relaxation and Parameters of Vogel−Fulcher−Tammann−Hesse Equation for PDBM25, PDBM23, and PDBM34

sample	PDBM23	PDBM25	PDBM34
$E_{a,\gamma'}$ (kJ mol^{-1})	54 ± 1	73 ± 2	39 ± 5
$E_{a,\gamma}$ (kJ mol^{-1})	95 ± 2	104. ± 3	80 ± 4
$E_{a,\beta}$ (kJ mol^{-1})	132 ± 2	138 ± 4	168 ± 3
$E_{a,\sigma}$ (kJ mol^{-1})	126 ± 2.0	136 ± 4	167 ± 3
D_0	6.1 ± 1.8	6.5 ± 1.2	6.7 ± 1.1
T_V (K)	265 ± 7	252 ± 11	271 ± 1
$10^2(\Phi_g/B)$	3.4 ± 0.9	3.5 ± 0.7	3.3 ± 0.6
$10^4\alpha_{f/B}$ (K^{-1})	6.2 ± 1.3	6.1 ± 1.3	5.5 ± 1.2

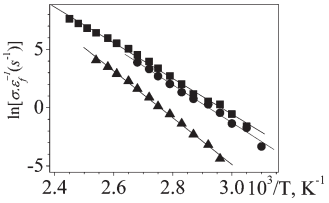

Figure 13. Dependence of the ionic conductivity with the temperature for PDBM23 (■), PDBM25 (●) and PDBM34 (▲).

worth noting that T_V is about 50 K below the T_g of the polymers. By comparing eq 9 with the Doolittle equation[41]

$$\tau_\alpha = \tau_0 \exp\left(\frac{B}{\Phi}\right) \tag{10}$$

where Φ is the relative free volume and B is a parameter close to the unit related with ratio between the critical volume necessary for a relaxation process to take place and the volume of the segments intervening in the relaxation, it is found that the relative free volume at T_g, Φ_g, and the thermal expansion coefficient $\alpha_f = (1/\nu)(d\nu/dT)_p$ are given by[42]

$$\Phi_g/B \cong \frac{T_g - T_V}{D_0 T_V}; \quad \alpha_f/B \cong 1/(D_0 T_V) \tag{11}$$

The fact that the ratio of constant volume to constant pressure activation energies for polymers is not zero[15] as free volume theories require raises questions concerning the applicability of these theories to α relaxations. However, it is an experimental fact that the values of the parameters Φ_g/B and α_f/B for most flexible polymers lie in the vicinities of 0.025 ± 0.005 and $(4-6) \times 10^{-4}$ K^{-1}. For PDBM23, PDBM25, and PDBM34 the values of Φ_g/B, collected in Table 1, are slightly higher than the indicated average value of this quantity, but the results for $\alpha_{f/B}$, also shown in Table 1, are in agreement with those reported for other flexible polymers[42] which lie in the vicinity of 5×10^{-4} K^{-1}.

The Arrhenius plot for the retardation time of the α′ relaxation of PDBM23, shown in Figure 12, suggests that the absorption may not be a pure thermal activated process. However, the fact that the data available cover a relatively narrow span of temperature impedes to reach a definite conclusion concerning the temperature dependence of this relaxation.

The values of the ionic conductivity obtained by minimization of eq 5 are plotted as a function of the reciprocal of temperature in Figure 13. The plots show that the conductivity of the polymers obeys Arrhenius behavior following the trends σ(PDBM23) > σ(PDBM25) > σ(PDBM34). The values of the activation energy associated with the ionic transport of the polymers, shown in the fourth row of Table 1, are of the same order as those associated with the β relaxation process of the polymers.

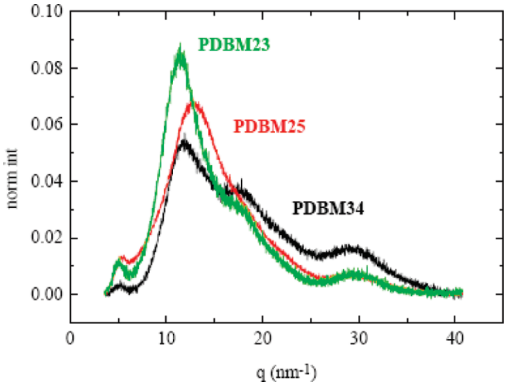

Figure 14. X-ray diffraction pattern for PDBM23 (green), PDBM25 (red), and PDBM34 (black).

4. Discussion

For polymers having dipole moment components in the side groups that can move without necessarily involving motions of the chain backbone, dipoles of type C according to Stockmayer's nomenclature, the dipole moment $\boldsymbol{\mu}$ and the end-to-end distance $\mathbf{r}$ of the chains are uncorrelated, i.e.[43]

$$\langle \boldsymbol{\mu} \cdot \mathbf{r} \rangle = 0 \tag{12}$$

Uncorrelation between dipole moment and end-to-end distance also occurs in polymers having dipoles rigidly attached to the backbone but perpendicular to the chain contour (dipoles of type B). However, for polymers with dipoles parallel to the chain contour (dipoles of type A), the dipole moment of the chain is correlated with the end to end distance, i.e.[43]

$$\langle \mu \cdot \mathbf{r} \rangle = \text{const} \langle r^2 \rangle \tag{13}$$

These latter polymers present the normal mode reflecting chains disentanglement that appears at lower frequencies than the α relaxation. Owing to the fact that the dipoles of PDBM23 are of type C, the α′ relaxation is not associated with long-range motions of the molecular chains. The α′ relaxation could be attributed to the fact that the PDBM23 used in the experiments is a mixture of two polymers, but the NMR spectrum of the polymer and the DSC thermogram rule out this possibility.

X-ray diffraction patterns of poly(*n*-alkyl methacrylate)s (PnMAs) show the aggregation of the side groups of different monomeric units forming self-assembled alkyl nanodomains[8,10] whose sizes depend on the side-chain length. The two glass transition temperatures detected in these polymers by dynamic heat capacity measurements are believed to be associated with the freezing of motions within the alkyl nanodomains (α_{PE}) and main-chain dynamics. By using neutron scattering with isotopic labeling, Arbe et al.[44] were able to study separately the dynamics of the alkyl nanodomains and the main chain. The results obtained strongly support the suggested nanosegregation of side groups and main chain.[8] Structural studies carried out by WAXS on the polymers used in this work, presented in Figure 14, show the presence of a peak, centered in the vicinity of $q = 5$ nm^{-1} (peak I), and a second peak (peak II) centered at $q = 11.5$, 12.1, and 13.8 nm^{-1} for PDBM23, PDBM34, and PDBM25, respectively.[45] Peak II also appears in PnMAs, centered in the vicinity of 12−13 nm^{-1}. The fact that this high-q peak is nearly independent of the side-chain length in PnMAs led to conclude that it is produced by correlations involving the side group atoms, thus reflecting the average distance between the nonbonded atoms of the side chains. According to this interpretation and taking into account the Bragg approximation, the average distance of the side chains

in PDBM23, PDBM25, and PDBM34 is respectively 0.55, 0.52, and 0.49 nm. Peak I also appears in PnMAs for values of q lying in the range 6, 5, and 4 nm^{-1} for poly(ethyl methacrylate), poly(butyl methacrylate), and poly(hexyl methacrylate). The shifting of peak I to lower values of q as the length of the alkyl chains increases suggests that it reflects main-chain correlations, and therefore it is associated with average distances between the backbone. In consonance with this, it can be assumed that peak I in the diffraction patterns of the dimethoxyphenyl-substituted poly(benzyl methacrylate)s also arises from main-chain correlations. Then, it could be postulated the existence of side-chain nanodomains flanked by the backbone in the polymer melts, the average distance between the backbone being ca. 1.26 nm. Accordingly, interfaces in the nanodomains of PDBM23, PDBM25, and PDBM34 may condition charge transport in the polymers melts at low frequencies, as discussed below.

An inspection of the retardation spectra shows that in addition to the high-frequency absorptions comprising the secondary and the glass−rubber relaxations processes arising from either interfacial and/or electrode polarization must be considered. Electrode polarization proceeds from accumulation of charges at the electrodes−polymer interface whereas the interfacial polarization is due to the buildup of charges at the interfaces of components of heterogeneous systems.[46] The contribution to the dielectric loss of the polarization produced at the electrodes−polymer interface scales with frequency as ω^{-s}, where s is a parameter close to the unit. This contribution corresponds to the last term of the right-hand side of eq 1. The interfacial polarization in the bulk is known as Maxwell−Wagner−Sillars (MWS) relaxation.[47−52] For example, MWS relaxations have been found in silicon−polyester resins,[44] nylon/clay nanocomposites,[52,53] PZTfibers/epoxy resins,[54] polycarbonate/styrene−acrylonitrile copolymer multilayer composite,[55] amorphous−crystal interface in nylon-1010,[56] etc. The MWS relaxation is associated with polarization processes produced by charges separated over a considerable distance with respect to the atomic or segments size. In view of these antecedents, the MWS polarization of PDBM23 may be interpreted as caused by nanoheterogeneities arising from the two types of environments existent in this apparently homogeneous system. However, the sizes of the nanodomains are not large enough or the polar side groups are not sufficiently flexible to develop cooperative motions independently of the backbone. It is worth noting that cooperative motions of the side chains of the higher series of poly(n-alkyl methacrylate)s produce a low-temperature glass−rubber (α_{PE}) relaxation, in addition to the glass rubber absorption arising from segmental motions of the backbone.[10] Although the symmetry of the α′ relaxation in PDBM23 fulfills one of the requirements of MWS relaxations, the process is not described by a single relaxation time. This means that the α′ absorption is a distributed MWS relaxation produced by a wide variety of environments. The isotherms corresponding to the real component of the complex conductivity of these nanoheterogeneous systems are characterized by a plateau in the low-frequency region and a critical frequency ω_c describing the onset of the dispersion of σ'. Empirically, it has been found that $\omega_c \cong \omega_M$ for a series of systems where ω_M is the angular frequency at the peak maximum of the dielectric loss. Charge transport in these systems can be interpreted in terms of a random barrier model proposed by Dyre[57,58] which assumes that transport occurs by hopping of charge carriers in spatially varying random energy landscape. The time involved in overcoming the highest barrier that determines the conductivity is one of the parameters characteristic of the model, denoted by τ_e. The Dyre model approximates the complex dielectric permittivity by the following expression

$$\varepsilon^*(\omega) = \varepsilon_0 + \frac{\sigma_0 \tau_e}{\varepsilon_f \ln(1+\omega\tau_e)} \qquad (14)$$

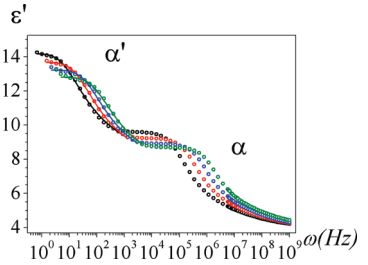

Figure 15. Fitting of the Dyre model (continuous lines) to the experimental real component of the complex dielectric permittivity from 378 to 408 K, at 10 K steps.

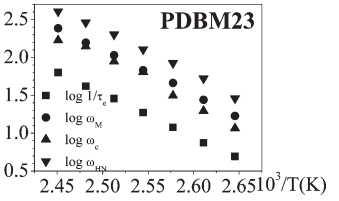

Figure 16. Arrhenius plots for the ω_c, ω_M, ω_{HN}, and ω_e parameters (see text for details).

where ε_0 is the relaxed value of the glass rubber relaxation and σ_0, the dc conductivity, is one of the characteristic parameters of the model. Taking into account that $(1+j\omega\tau_e) = (1+\omega^2\tau_e^2)^{1/2} e^{j\tan^{-1}(\omega\tau_e)}$, the real and imaginary components of ε^* are given by

$$\varepsilon'(\omega) = \varepsilon_{sd} + \frac{1}{2}\frac{\left(\frac{\sigma_0}{\varepsilon_f}\right)\omega\tau_e \ln(1+\omega^2\tau_e^2)}{(1/4)\ln(1+\omega^2\tau_e^2) + [\tan^{-1}(\omega\tau_e)]^2}$$
$$\varepsilon''(\omega) = \frac{1}{2}\frac{\left(\frac{\sigma_0}{\varepsilon_f}\right)\omega\tau_e \tan^{-1}(\omega\tau_e)}{(1/4)\ln(1+\omega^2\tau_e^2) + [\tan^{-1}(\omega\tau_e)]^2} \qquad (15)$$

Notice that the model is not applicable at very low frequencies where electrode polarization effects show up because these effects are not considered in the model. As can be seen in Figure 15, eq 15a fits rather well to the ε' isotherms of PDBM23 in the low-frequency range provided that the values of σ_0 and ω_e plotted as a function of the reciprocal of temperature in Figures 13 and 16, respectively, are used. Although the values of σ_0 are roughly a decade higher than those of σ plotted in Figure 13, the temperature dependences of both quantities are similar. As can be seen in Figure 16, the values of ω_c, ω_M, and ω_e apparently obey Arrhenius behavior, and the results for ω_c and ω_M nearly fall in the same curve, suggesting that they describe an identical underlying process, i.e., an electrical relaxation. As expected, the values of ω_e are rather close to those of ω_c and ω_M. Owing to the rather narrow span of temperature covered by the experiments where ω_M, ω_c, and ω_e can be obtained, no definitive conclusion can be reached regarding to whether these parameters are only thermally activated or they are also governed by the volume; i.e., the temperature dependence of the parameters is described by the VFTH equation. It can be noted in this regard that the study of the temperature dependence of these parameters for low molecular weight ionic liquids carried out in a wide span of temperature show that they are governed by the temperature and volume.[59] The study of the ω_c, ω_M, and ω_e ($1/\omega_e$) dependence with temperature has only been made for the PDBM23 because in the case of PDBM25 and PDBM34 the experimental frequency does not reach low enough values to get a clear view of the process under study.

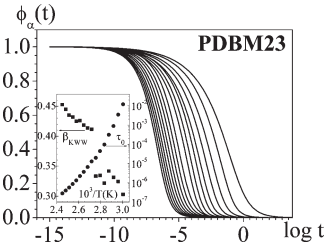

Figure 17. Normalized relaxations curves in the time domain for the α relaxations of PDBM23 from 363 to 408 K, at 5 K steps. Inset: temperature dependence of the stretch exponents β_{KWW} and the characteristic relaxation times τ_0 of the KWW equation of PDBM23.

To asses the influence of the fine structure on the stretch exponent of the decay function that describes the glass−rubber relaxation, the normalized α relaxation in the time domain was calculated from the spectra by means of the equation

$$\phi(t) = \frac{\int_{-\infty}^{\infty} L_\alpha(\ln \tau) e^{-t/\tau} \, d \ln \tau}{\int_{-\infty}^{\infty} L_\alpha(\ln \tau) \, d \ln \tau} \quad (16)$$

The normalized decay function that depicts the relaxation behavior of PDBM23 in the whole time range was calculated from the retardation spectra by means of eq 16. The decay functions obtained for PDBM23 at different temperatures are shown in Figure 17. As usual, the decay function is inevitably described by the stretch exponential KWW equation[16]

$$\phi(t) = \exp\left[-\left(\frac{t}{\tau_0}\right)^{\overline{\beta}}\right] \quad (17)$$

where $0 < \overline{\beta} \leq 1$ and τ_0 is the characteristic relaxation time of the absorption. Values of the evolution of the stretch exponent and the characteristic relaxation time with temperature for PDBM23 are depicted in Figure 17. The decay curves for the rest of polymers are given in Figure 5 of the Supporting Information. As expected, the temperature dependence of τ_0 obeys the VFTH equation, whereas the stretch exponent seems to increase as temperature increases. The three polymers exhibit rather low stretch exponents at low temperature that increase with increasing temperature, without observing differences in behavior that that can be attributed to the small variations of the fine structure of the polymers.

The rapidity with which the physical properties of a supercooled liquid varies as temperature approaches the glass transition temperature is characterized by the dynamic fragility m given by[60,61]

$$m = \lim_{t \to \infty} \left(\frac{d \log \xi}{d(T_g/T)}\right)_p \quad (18)$$

where ξ is a physical parameter depending of the dynamics of the system such as the viscosity η or the relaxation time τ. Obviously, as the fragility parameter increases, the temperature dependence of the relaxation time of the glass−rubber relaxation comes closer to Arrhenius behavior. Taking τ_g as reference and taking into account eq 9, the fragility parameter can be written as

$$m = \frac{D_0 T_V}{2.303 T_g (1 - T_V/T_g)^2} \quad (19)$$

The values of m for PDBM23, PDBM25, and PDBM34, collected in Table 2, slightly increase with the respective glass transition temperatures. However, the results are nearly 30% below those predicted by the straight line roughly fitting the values of m vs T_g for several polymers.[61] The apparent activation energy associated with the α relaxation at T_g can be obtained by equating the fragility index obtained from VFTH and Arrhenius behavior, i.e.

$$m = \left[\frac{d \log \tau_A}{d \log(T_g/T)}\right]_{T=T_g} = \left[\frac{d \log \tau_{VFTH}}{d \log(T_g/T)}\right]_{T=T_g} \quad (20)$$

Taking into account that $\tau_A = \exp(-E/RT)$, eq 20 leads to the following expression for the activation energy E_α at T_g

$$E_\alpha(T_g) = \frac{R D_0 T_V}{(1 - T_V/T_g)^2} \quad (21)$$

From eqs 21 and 18, the activation energy can be expressed by the alternative form

$$E_\alpha(T_g) = 2.303 R D_0 T_V T_g \quad (22)$$

Accordingly, the higher T_g, the higher the activation energy, assuming D_0 and T_V as constants. The results for the activation energy associated with the glass−rubber relaxation of PDBM23, PDBM25, and PDBM34 at T_g, collected in Table 2, increase with temperature but lie about 25% below those[61] predicted by the straight line roughly fitting the plots of $E_{a,\alpha}(T_g)$ vs T_g for a wide variety of polymers.

Aside from other procedures, a method to collect the behavior of a variety of systems with temperature in a single diagram is to consider the β relaxation, which obeys Arrhenius behavior, the elementary relaxation for the α relaxation of liquids.[62] Using this assumption, the α relaxation can be considered associated with an activation energy that depends on temperature. Then the ratio between the activation energy of the α relaxation at a temperature T and that of the β absorption, independent of temperature, may represent the size of correlate domains in the α relaxation. The ratio, represented by $R_\alpha(T)$, can be written as[62]

$$R_\alpha(T) = \frac{R D_0 T_V T^2}{E_\beta (T - T_V)^2} \quad (23)$$

It can be defined a temperature T_B at which $R_\alpha(T) = 1$ representing the upper bound below which the size of correlate domains starts to increase reaching a maximum at $T = T_g$. The values of T_B for PDBM23, PDBM25, and PDBM34 are 388.3, 362.7, and 395.0 K, respectively. The variation of the size of correlate domains with temperature, shown in Figure 18, indicates that the correlated domains of PDBM23, PDBM25, and PDBM34, at the respective glass transition temperatures, are respectively, 3.4, 2.7, and 3.1 times the size of the elementary clusters at T_B.

A few comments should be made concerning the assignment of the secondary absorptions to specific molecular motions of the

Table 2. Values of the Glass Transition Temperature (T_g), the Dynamic Fragility Index (m), and the Activation Energy Associated with the α Relaxation at T_g, $E_\alpha(T_g)$, for PDBM23, PDBM25, and PDBM34[a]

sample	PDBM23	PDBM25	PDBM34
T_g, K	320	310	330
m	74	66	74
m*	99	96	101
$E_\alpha(T_g)$, kJ mol^{-1}	451	390	467
E_α*(T_g), kJ mol^{-1}	579	541	618

[a] The quantities with an asterisk, m* and E_α*(T_g), were calculated by empirical equations given in ref 61 (m* ≈ 0.28(±0.067)T_g (K) + 9(±20); E_α*(T_g) = [0.006T_g^2 (K) − 35] kJ/mol).

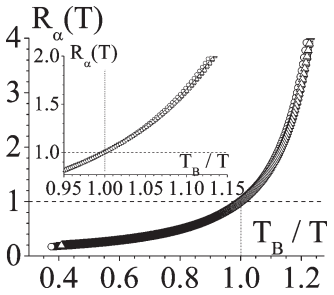

Figure 18. Temperature dependence of ratio of the activation energy of α process to that of β process, $R_\alpha(T)$, for PDBM23 (squares), PDBM25 (circles), and PDBM34 (triangles).

side groups. The $CC(O)-OCHH_2$ residue of the side chain is associated with a dipole moment of 1.78 D, forming an angle of 123° with the C−C(O)O bond.[63] On the other hand, the dipole associated with the $C^{ar}-O-CH_3$ moiety bisects the $C^{ar}-O-C$ angle and has a value of 1.22 D.[63] With the exception of the bonds restricted to trans states, rotations about the remaining skeletal bonds of the side groups, including the $C^{ar}-O-CH_3$ bonds, give rise to dielectric activity. However, coplanarity between the phenyl group and the $C^{ar}OCH_3$ moiety is strongly disfavored due to strong repulsive interactions between the methyl group and nearby protons of the phenyl group. Then dipoles jumping between the two alternative gauche states about the $C^{ar}-OCHH$ bonds presumably produce the dielectric activity displayed in the fastest relaxation or γ' process. On the other hand, rotations about the $C^{ar}-CH_2$ bonds change the location in the space of the dipoles associated with the $C^{ar}-OCHH_3$ moiety, probably producing the dielectric activity reflected in the γ relaxation. In this case jumping between the two lower energy planar conformations about the $C^{ar}-CH_2$ bonds presumably produces that relaxation. Finally, the β relaxation arises from motions involving the whole side group presumably coupled with local motions of the skeletal bonds of the main chain. In general, the conformations of lower energy of the side groups of the chains with the $C^{ar}-O-CH_3$ bonds anchored to the position 2 of the phenyl group have the dipole associated with this moiety in a direction forming favorable angles with the dipole corresponding to the ester group. Hence, the high dielectric strength is produced by the motions of the side chains of PDBM23 and PDBM25. The angles formed by the dipoles of the $C^{ar}-O-CH_3$ bonds in 3,4 positions with the dipole of the ester groups are not so favorable and as a result the dielectric strength of PDBM34 is significantly lower than that of the other polymers.

5. Conclusions

The dielectric loss isotherms of the polymers in the frequency domain present a blurred relaxation resulting from the overlapping of the secondary absorptions with the glass−rubber (α) relaxation. The time retardation spectra computed from the complex dielectric permeability allow a better deconvolution of overlapping relaxations than performing directly the deconvolutions in the dielectric loss. A distributed MWS relaxation appears at long times in the retardation spectra at high temperatures hidden in the dielectric loss spectra by the interfacial polymer−electrode conductive contribution to the dielectric loss. The MWS relaxation presumably arises from the buildup of charges at the interfaces of nanoheterogeneities formed in the bulk by segregation of the polar side groups from the nonpolar skeletal bonds. This relaxation is described by the Dyre model, which assumes that charge transport occurs by hopping of charge carriers in spatially varying random energy landscape. The location of the polar oxymethylene substituents on the phenyl groups of the side chains greatly influences the relaxation behavior of the polymers. The location of the oxymethylene moiety in the position 2 of the phenyl group causes a significant enhancement of the dielectric strength of the relaxations. This study shows that small differences in the fine structure of polymers produce significant changes in the relaxation behavior.

Acknowledgment. This work was financially supported by the DGCYT and CAM through Grant MAT2008-06725-C03. D.R. and L.G. thank Fondecyt, Grants 1080007 and 1080026, for partial financial help.

Supporting Information Available: RMN characterization of the monomers and polymers and several figures with the experimental results and dielectric characterization of materials analyzed. This material is available free of charge via Internet at http://pubs.acs.org.

References and Notes

(1) Ishida, Y.; Yamafuji, K. *Kolloid Z.* **1961**, *177*, 97.
(2) (a) Williams, G. *Trans. Faraday Soc.* **1964**, *60*, 1556. (b) McCrum, N. G.; Read, B. E.; Williams, G. *Anelastic Effects in Polymeric Solids*; Wiley: New York, 1967.
(3) Sasabe, H.; Saito, S. *J. Polym. Sci., Part A2* **1968**, *6*, 1401.
(4) Ishida, Y. *J. Polym. Sci., Part A2* **1969**, *7*, 1835.
(5) Kuebler, S. C.; Schaefer, D. J.; Boeffel, C.; Pawelzik, U.; Spiess, H. W. *Macromolecules* **1997**, *30*, 6597.
(6) Floudas, G.; Stepanek, P. *Macromolecules* **1998**, *31*, 6951.
(7) Schroter, K.; Unger, R.; Reissig, S.; Garwe, F.; Kahle, S.; Beiner, M.; Donth, E. *Macromolecules* **1998**, *31*, 8966.
(8) (a) Beiner, M.; Kahle, S.; Abens, S.; Hempel, E.; Höring, S.; Meissner, M.; Donth, E. *Macromolecules* **2001**, *34*, 5927. (b) Beiner, M.; Huth, H. *Nature Mater.* **2003**, *2*, 595.
(9) Gómez, D.; Alegría, A.; Arbe, A.; Colmenero, J. *Macromolecules* **2001**, *34*, 503.
(10) Beiner, M. *Macromol. Rapid Commun.* **2001**, *22*, 869.
(11) Wind, M.; Graf, R.; Heuer, A.; Spiess, H. W. *Phys. Rev. Lett.* **2003**, *91*, 155702–I.
(12) Wind, M.; Graf, R.; Renker, S.; Spiess, H. W. *J. Chem. Phys.* **2005**, *122*, 014906.
(13) Ngai, K. L.; Gopalkrishnan, T. R.; Beiner, M. *Polymer* **2006**, *47*, 7222.
(14) Arbe, A.; Genix, A.-C.; Colmenero, J.; Richter, D.; Fouquet, P. *Soft Matter* **2008**, *4*, 1792.
(15) Mpoukouvalas, K.; Floudas, G.; Williams, G. *Macromolecules* **2009**, *42*, 4690.
(16) Williams, G. *Adv. Polym. Sci.* **1979**, *33*, 60.
(17) Kremer, F., Schönhals, A. In *Broadband Dielectric Spectroscopy*; Springer: Berlin, 2003.
(18) Floudas, G. *Prog. Polym. Sci.* **2004**, *29*, 1143.
(19) Williams, G. *Trans. Faraday Soc.* **1966**, *6*, 2091.
(20) Beiner, M.; Huth, H. *Nature Mater.* **2003**, *2*, 595.
(21) Díaz-Calleja, R.; Sanchis, M. J.; Saiz, E.; Martínez Piña, F.; Miranda, R.; Gargallo, L.; Radic, D.; Riande, E. *J. Polym. Sci., Polym. Phys. Ed.* **2000**, *38*, 2179.
(22) Domínguez-Espinosa, G.; Riande, E.; Díaz-Calleja, R.; Gargallo, L.; Radic, D. *J. Chem. Phys.* **2005**, *123*, 114904.
(23) Domínguez-Espinosa, G.; Díaz-Calleja, R.; Riande, E.; Gargallo, L.; Radic, D. *Macromolecules* **2006**, *39*, 3071.
(24) Domínguez-Espinosa, G.; Díaz-Calleja, R.; Riande, E. *Macromolecules* **2006**, *39*, 5043.
(25) Díaz-Calleja, R.; Domínguez-Espinosa, G.; Riande, E. *J. Non-Cryst. Solids* **2007**, *353*, 719.
(26) Sanchis, M. J.; Domínguez-Espinosa, G.; Díaz-Calleja, R.; Guzmán, J.; Riande, E. *J. Chem. Phys.* **2008**, *129*, 54903–15.
(27) Burtle, G. J.; Turek, W. N. *J. Org. Chem.* **1954**, *19*, 1567.
(28) Gargallo, L.; Muñoz, M. I.; Radić, D. *Polymer* **1986**, *27*, 1416.
(29) Havriliak, S.; Havriliak, S. J. *Dielectric and Mechanical Relaxation in Materials*; Hanser: Munich, 1997; p 57.
(30) McCrum, N. G.; Read, B. E.; Williams, G. *Anelastic and Dielectric Effects in Polymeric Solids*; Wiley: London, 1967; Chapter 4.
(31) Riande, E.; Díaz-Calleja, R. *Electrical Properties of Polymers*; Dekker: New York, 2004; Chapter 8.
(32) Domínguez-Espinosa, G.; Ginestar, D.; Sanchis, M. J.; Díaz-Calleja, R.; Riande, E. *J. Chem. Phys.* **2008**, *129*, 104513.

(33) (a) Press, W. H.; Teukolsky, S. A.; Vetterling, W. T.; Flannerty, B. P. In *The Art of Scientific Computing*, 2nd ed.; Cambridge University Press: New York, 1992; Chapter 18. (b) Morozov, V. A. *Methods for Solving Incorrectly Posed Problems*; Springer: New York, 1984.
(34) Havriliak, S.; Negami, S. *J. Polym. Sci., Polym. Symp.* **1966**, *14*, 99.
(35) Zorn, R. *J. Polym. Sci., Part B: Polym. Phys.* **1999**, *37*, 1043.
(36) Vogel, H. *Z. Phys.* **1921**, *22*, 645.
(37) Fulcher, G. S. *J. Am. Ceram. Soc.* **1925**, *8*, 339.
(38) Tammann, G.; Hesse, W. *Z. Anorg. Allg. Chem.* **1926**, *156*, 245.
(39) Angell, C. A. In *Complex Behavior of Glassy Systems*; Proceedings of the XIV Sitges Conference, Sitges, Barcelona, Spain, 10−14 June 1996; Rubi, M., Pérez-Vicente, C., Eds.; Springer: Berlin, 1997.
(40) Angell, C. A. *Science* **1995**, *262*, 1924.
(41) (a) Doolittle, A. K. *J. Appl. Phys.* **1951**, *22*, 1471. (b) Doolittle, A. K. *J. Appl. Phys.* **1952**, *23*, 236.
(42) Ferry, J. D. *Viscoelastic Properties of Polymers*, 2nd ed.; John Wiley & Sons: New York, 1961.
(43) Stockmayer, W. H. *Pure Appl. Chem.* **1967**, *15*, 539.
(44) Arbe, A.; Genix, A.-C.; Colmenero, J.; Richter, D.; Fouquet, P. *Soft Matter* **2008**, *4*, 1792.
(45) In principle, tacticity may affect the crystallinity of poly(methacrylate) derivatives and therefore their X-ray patterns. Actually, iso-poly(methyl methacrylate) develops crystalline order from the melt, and the same occurs with syndio-poly(methyl methacrylate), but in this latter case only from solution (Davis, T. P. Polyacrylates. In *Polymer Handbook*; Olabisi, O., Ed.; Marcel Dekker: New York, 1997; Chapter 10). However, development of crystallinity in iso-poly(methyl methacrylate) melts is slow, even for a nearly monodisperse sample with isotactic triad content of 100%. Crystallinity is not obtained in samples with isotactic content triad less than 53% (Lemieux, E.; Prud'homme, R. E. *Polym. Bull.* **1989**, *21*, 621). In view of this and taking into account the atactic nature of PDBM23, PDBM25, and PDBM34, crystalline order arising from estereoregularity is absent in these polymers.
(46) Satti, G.; McLachlan, D. S. *J. Mater. Sci.* **2007**, *42*, 6477.
(47) Laredo, E.; Herandez, M. C. *J. Polym Sci., Part B: Polym. Phys.* **1997**, *35*, 2879.
(48) Maxwell, J. C. *Electricity and Magnetism*; Clarendon: Oxford, 1893.
(49) Wagner, K. W. *Arch. Elektrotech.* **1914**, *2*, 371.
(50) Sillars, R. W. *Inst. Electr. Eng.* **1937**, *80*, 378.
(51) Mijovic, J.; Fitz, B. D. *Novocontrol Applic Note Dielectrics* **1998**, *26*.
(52) Perrier, G.; Bergeret, A. *J. Polym Sci., Part B: Polym. Phys.* **1997**, *35*, 1349.
(53) Lee, Y-H.; Bur, A. J.; Roth, S. C.; Start, P. R. *Macromolecules* **2005**, *38*, 3828.
(54) Hammami, H.; Arous, M.; Lagache, M.; Kallel, A. *J. Alloys Compd.* **2007**, *430*, 1.
(55) Daly, J. H.; Guest, M. J.; Hayward, D.; Pethrick, R. A. *J. Mater. Sci., Lett.* **1992**, *11*, 1271.
(56) Lu, H.; Zhang, X. J. *Macromol. Sci. Phys.* **2006**, *45*, 933.
(57) Dyre, J. C. *J. Phys. C: Solid State Phys.* **1986**, *19*, 5655.
(58) Dyre, J. C. *J. Appl. Phys.* **1988**, *64*, 5.
(59) Krause, C.; Sangoro, J. R.; Kremer, F. *J. Phys. Chem. B* **2010**, *114*, 382.
(60) Plazek, D. J.; Ngai, K. L. *Macromolecules* **1991**, *24*, 1222.
(61) Qin, Q.; McKenna, G. *J. Non-Cryst. Solids* **2006**, *352*, 2977.
(62) Fujimori, H.; Oguni, M. *Solid State Commun.* **1995**, *94*, 157.
(63) Riande, E.; Saiz, E. *Dipole Moments and Birefringence of Polymers*; Prentice Hall: Englewood Cliffs, NJ, 1992.